INTENSE NON-LINEAR SOFT X-RAY EMISSION FROM A HYDRIDE TARGET DURING PULSED D BOMBARDMENT

GEORGE H. MILEY, YANG YANG, ANDREI LIPSON, MUNIMA HAQUE, AND IAN PERCEL

Department of Nuclear, Plasma and Radiological Engineering, University of Illinois, 103 S. Goodwin Ave., Urbana, IL 61801, U.S.A.

MICHAEL ROMER

Department of Electrical and Computer Engineering, University of Illinois, 1406 W. Green St., Urbana, IL 61801, U.S.A.

Radiation emission from Low Energy Nuclear Radiation (LENR) electrodes (both charged-particle and x-rays) represents an important feature of LENR in general. Here, calibration, measurement techniques, and soft x-ray emission results from deuterium bombardment of a Pd target (cathode) placed in a pulsed deuterium glow discharge (PGD) are described. An x-ray intensity of 13.4 mW/cm^2 and a dose of 3.3 $\mu J/cm^2$ were calculated over a 0.5 ms pulse time from AXUV photodiode radiation detector measurements. A most striking feature is that x-ray energies > 600 V are observed with a discharge voltage only about half of that value. To further investigate this phenomenon, emission during room temperature D-desorption from electrolytically loaded Pd:Dx cathodes was also studied. The x-ray emission energy observed was quite similar to the PGD case. However, the intensity in this case was almost 13 orders of magnitude lower due to the much lower deuterium fluxes involved.

1   Introduction

A. B. Karabut in the LUTCH Laboratory in Russia recently reported x-ray laser (~1.5 keV) emission from metal targets such as Ti and Pd, which served as the cathode in a high-current pulsed deuterium glow discharge plasma diode [1]-[2]. Later, he vividly demonstrated the potential capability of this type of laser with a small follow-up 10 W "prototype" unit, which "drilled" a 9-mm diameter hole in a 3-cm thick plastic target. This remarkable unit is more compact and provides a shorter wavelength than any prior "table top" x-ray laser. Staff at the University of Illinois at Urbana-Champaign (UIUC) have undertaken theoretical and experimental studies of the mechanisms involved in this unique x-ray emission phenomenon [2]-[3].

In UIUC's experiments, it was established that anomalous x-ray emission is observed during PGD operation at a pressure of 0.1-0.5 Torr and at a spacing of about 4.0 mm between the cathode and anode. The current pulses have a square shape with 0.2-2.0 ms duration and a rise time of 0.1 µs. The glow discharge operated at a voltage as low as 300 V with a pulsed current up to 2 A. These crucial conditions are similar to those in Karabut's earlier studies [1-2], but the voltage operation down to 300 V represents a new region.

This paper will briefly describe the UIUC pulsed deuterium bombardment glow discharge project. The x-ray diagnostics employed and their calibration will be discussed.

The calibration will be applied to discharge data to determine the power, intensity, dosage, and efficiency of the x-ray observed. Finally a brief discussion is given of related experiments using a deuterium flux created by desorption of D loaded in a Pd target electrolytically. These experiments have much lower D-fluxes than PGD, but low level x-ray production thought to be related to the discharge phenomenon.

2   Experimental Setup

UIUC staff have designed and fabricated a unique new type of discharge chamber (Figure 1) which contains a water-cooled cathode (the target can be mounted easily, and is capable of linear motion), a stainless steel anode (capable of angular motion), and a photodiode soft x-ray detector (which will be discussed in-depth shortly). A beryllium filter was placed in front of the detector to prevent detection of visible light. In order to reduce the electrical leakage current between the anode and the ground and to confine the plasma to a smaller volume, a glass tube is added to surround the electrodes, as shown in Figure 1. On both ends of the tube, plates covered by insulating material are used to provide a sealed boundary for the discharge. Steady state I-V curves obtained after the addition of the glass tube showed that the applied voltage increased by 50%. A hole of 1-cm diameter was drilled into one side of the tube to allow x-rays to reach the detector with minimum absorption.

(a)   (b)
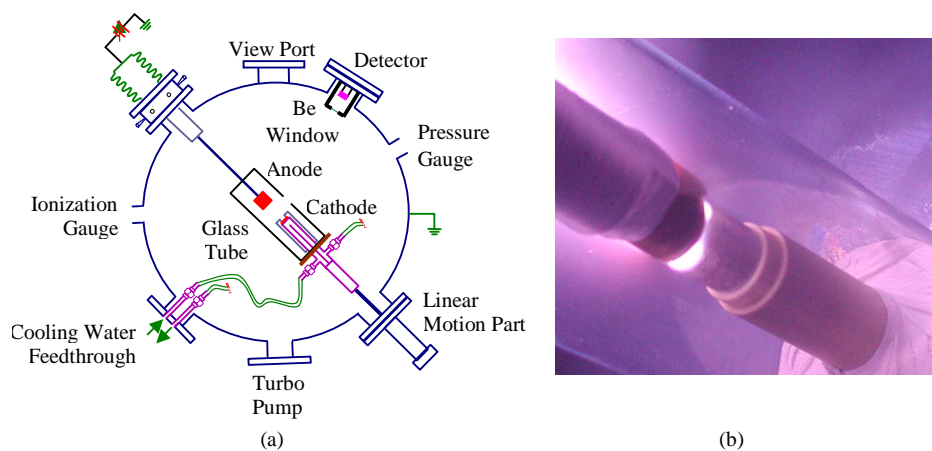
Figure 1. Experimental chamber diagram (a) and discharge view showing glass tube (b).

3   AXUV Detector Theory/Operation

The AXUV-100 detector is a silicon p-n junction photodiode that is well suited for the measurement of soft x-rays. Incoming photons or charged particles create electron-hole pairs in the junction of the photodiode. The total number of electron-hole pairs generated depends on the materials used in the photodiode and the incoming particle energy. For the AXUV, the average energy for electron-hole pair creation E_{e-h} is 3.7 eV [4]. However, phenomenons that also require some of the incident energy include "dead" doped regions

and surface recombination. The percentage of the total incident energy E_I going into electron-hole pairs is the "quantum efficiency" η_Q. Fortunately, the AXUV used has been engineered to approach theoretical quantum efficiency [4]. Thus, the number of electron-hole pairs is E_I divided by $E_{e\text{-}h}$. The p-n junction of the photodiode sweeps the electrons and holes across the junction and out through contacts. Thus, if the number of electron-hole pairs is known, the current they create can be calculated, or vice versa.

The measured current production characteristics of the AXUV are shown in Figure 2 [4]. The y-axis of Figure 2 is the responsivity of the photodiode, which is measured in amps per watt. With the responsivity information, it is simple to backtrack from the measured current to calculate the power incident on the detector. However, an oscilloscope was used to measure the voltage created. Thus, a basic circuit consisting of the AXUV photodiode and the oscilloscope is needed to understand the measurement (Figure 3).
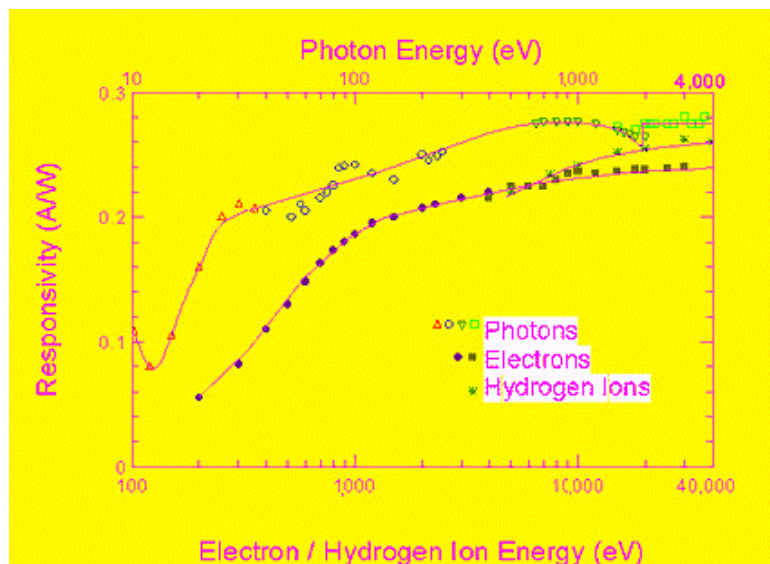

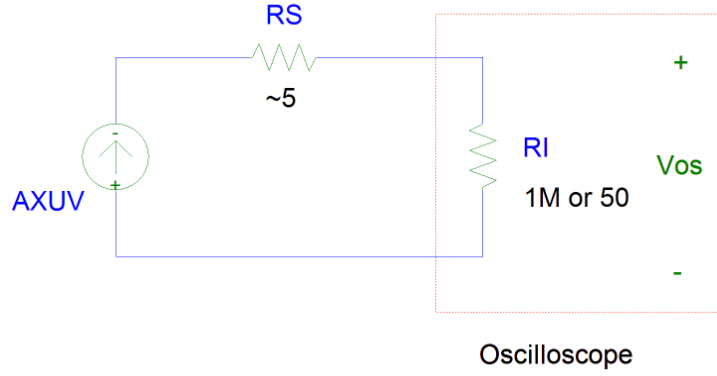Figure 2. AXUV photodiode responsivity in amps per watt [4].

Figure 3. Basic circuit of the AXUV (including a series resistance) and the oscilloscope.

As seen in Figure 3, the AXUV photodiode is modeled as a current source accompanied by an inevitable series resistance R_S—due to the silicon that the electrons and holes must travel through to escape. The series resistance is assumed to be 5 Ω [4]. The oscilloscope has an input resistance R_I which can be set at either 1 MΩ or 50 Ω. In the AXUV setup, the voltage read by the oscilloscope is

$$V_{Os} = I_{AXUV} R_I \qquad (1)$$

where I_{AXUV} = the current generated by the AXUV photodiode. The fraction of the total current that this corresponds to is

$$f_{I_{AXUV}} = \frac{R_I}{R_I + R_S}. \qquad (2)$$

Equations (1) and (2) show that a large input resistance R_I gives a high amplification, hence an accurate reading. However, the photodiode is a capacitive device, and the rise time of its response is directly proportional to the resistance it is discharged over:

$$\tau = 2.2(R_S + R_I)C \qquad (3)$$

where C = the capacitance of the photodiode [4].

The capacitance depends on the detailed photodiode properties, but a 4 pF value is assumed here. The fraction of the measured current and rise time calculation results for the 1 MΩ oscilloscope input resistance are given in Table 1.

Table 1: Current measurement fraction and rise time calculations for the high oscilloscope input resistance.

Parameter	Symbol	Units	Value
Series resistance	R_S	Ω	5
Oscilloscope high input resistance	$R_{I\text{-}High}$	Ω	10^6
Photodiode capacitance	C	pF	4
Fraction of measured current	$f_{I\text{-}1M\Omega}$		~1.00
Rise time	$\tau_{1M\Omega}$	s	8.8 x 10^{-6}

As seen, the theoretical rise time for the 1 MΩ R_I is rather large (microseconds). However, the other option, i.e. the 50 Ω input resistance, reduces the fraction of the total current measured. For the initial experiments here, we elected to use the 1 MΩ resistance to retain accuracy while sacrificing to some extent the time resolution. Since the x-ray output measurement duration is in the millisecond range, a rise/fall time of several microseconds should give reasonable detail.

4   Calibration

The calibration of the AXUV photodiode was done with a 7.5 mCi carbon-14 source. Carbon-14 is a beta emitter with average beta energy E_β of 49.5 keV [5]. Although ^{14}C is a beta source rather than an x-ray source, responsivity data is available up to 30 keV for electrons. While this is 20 keV short of E_β, the scale of Figure 2 is logarithmic, and the electron responsivity slope at the highest graphed energy is nearly flat. Responsivity data from Figure 2 is extrapolated to the energy of ^{14}C in Table 2. If the measurement techniques for ^{14}C are accurate, they should also be accurate for soft x-rays; the only difference being the responsivity of the AXUV.

Table 2. Electron responsivity data near $E_\beta = 49.5$ keV [4].

Electron Energy (keV)	Responsivity (A/W)
15	0.237
20	0.238
30	0.240
50	0.244 (extrapolated)

To match the measured results with the source intensity, the power that the ^{14}C source delivers to the collector must first be calculated:

$$P_D = A \cdot E_\beta \cdot A_D \cdot \frac{1}{A_S} \ (W) \qquad (4)$$

where A = the source activity (decays/s), E_β = the average beta energy (J), A_D = the detector surface area (cm^2), and A_S = the beta source surface area (cm^2).

The oscilloscope voltage can then be calculated by

$$V_{Os} = \Re_{C14} \cdot P_D \cdot R_I \ \ (V) \tag{5}$$

where $\Re_{C14}$ = the responsivity of the AXUV for ^{14}C betas (A/W), P_D = the power delivered to the detector by the ^{14}C source (W), and R_I = the input resistance of the oscilloscope (Ω). The calculated oscilloscope voltage and associated parameters are given in Table 3 for comparison with measured values cited later.

To eliminate background light, the photodiode was placed in a container that blocked out light on all sides but the entrance. The detector head was faced away from the entrance to minimize the light. A 20 MHz low pass filter was used with the oscilloscope to reduce the noise to a μV magnitude. The ^{14}C source was then placed in the container and gently pressed against the detector face. Since the ^{14}C source completely covered the detector face, essentially no light reached the AXUV. Several consecutive measurements were taken to find a stable, reproducible signal. The final measurement gave a voltage of 2.70 ± 0.25 mV.

This result is about a fifth of the projected voltage in Table 3. However, a thin layer of glass covers the ^{14}C source, and this is thought to attenuate the emitted betas, resulting in the smaller measured voltage.

Table 3. Projected oscilloscope voltage V_{Os} for the 7.5 mCi ^{14}C source.

Parameter	Symbol	Units	Value
Activity	A	mCi	7.5
Average beta energy	E_β	keV	49.5
Detector surface area	A_D	cm^2	1.0
Source surface area	A_S	cm^2	38.3
Power delivered to the detector	P_D	nW	57.5
Responsivity to ^{14}C betas	$\Re_{C14}$	A/W	0.244
Projected oscilloscope voltage	V_{Os}	mV	14.0

5 Results from AXUV Photodiode X-ray Measurements

Representative x-ray power measurements read are shown in Figure 4. The first 'step' in the figure at about 0.04 V is the background signal caused by pickup from the pulsed power supply. The sharp spikes at the beginning and end of the second rise are attributed to the extended rise time of the photodiode (due to the 1 MΩ oscilloscope input resistance). The second sharp rise near the middle of the pulse is attributed to the x-ray emission. It demonstrates two very striking features. First is the delay before initiation. Second, as seen later (Figure 6), the x-ray energy must exceed 600 V (due to the Be filter on the detector). Yet the discharge voltage was only ~ 300 V. This confirms the very non-linear behavior of this unusual x-ray generation mechanism.

5.1 Solid Angle Considerations

For the solid angle calculation, it is assumed that the soft x-rays generated are between 0.5 and 2 keV. The average responsivity in this region is about 0.270 A/W. Next, the

fraction of the source x-rays that the detector 'sees' must be found. The cathode and anode were surrounded by a glass cylinder during the plasma experiment to prevent arcing problems. A hole drilled in one of the vertical sides of the cylinder allowed the x-rays to escape and be collected. A diagram of the glass cylinder/vessel system is shown in Figure 5. (The geometry leading to this setup is shown in Figure 1.)

The chord subtended by the hole was measured to be 400 mm. Then the total subtended angle θ_{TOT} is found to be 1.63 radians. To calculate the surface area of the vessel, hence detector, that this corresponds to, a solid angle surface area equation is used:

$$SA = r^2 \int\limits_0^\phi \int\limits_0^\theta \sin\phi \, d\phi \, d\theta = r^2 \int\limits_0^{\frac{1}{2}\theta_{TOT}} \int\limits_0^{2\pi} \sin\phi \, d\phi \, d\theta = r^2 \cdot 2\pi \cdot \left(1 - \cos\left(\frac{\theta_{TOT}}{2}\right)\right) \qquad (6)$$
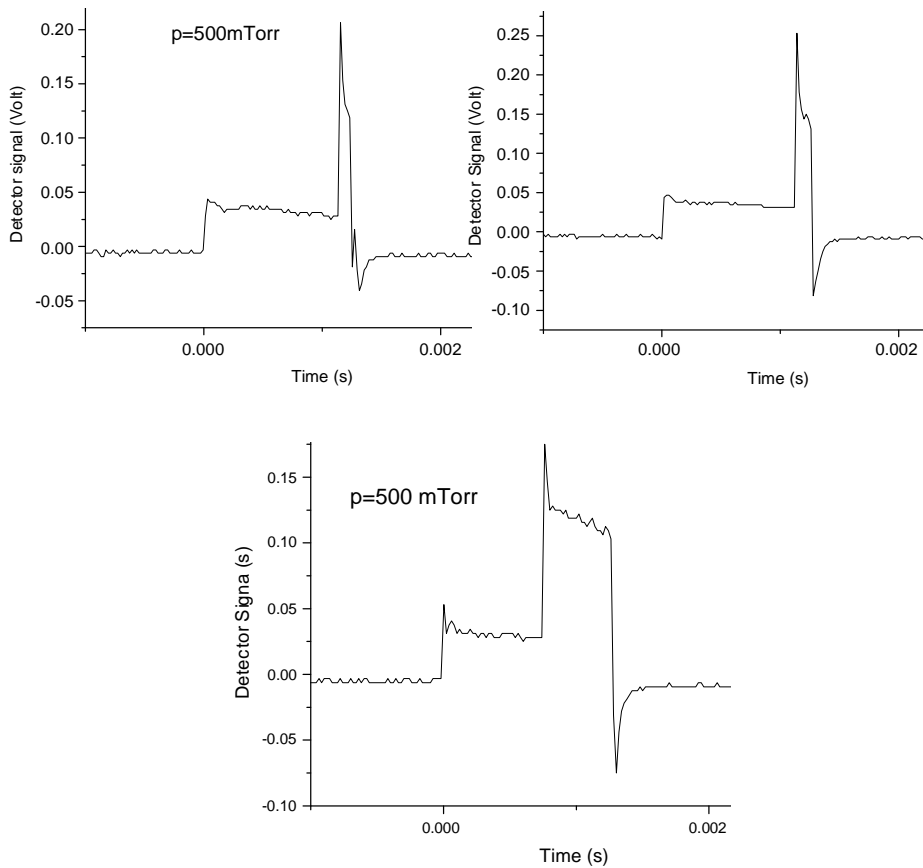
Figure 4. Three measurements of the x-ray emission pulse at 500 mTorr. Measurement 1 is the top left graph, measurement 2 is the top right, and measurement 3 is on the second row.
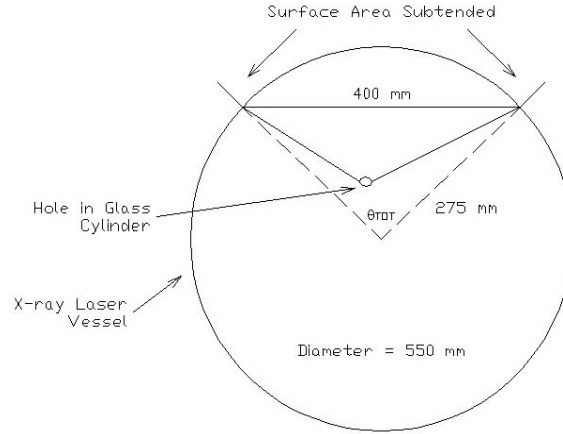
Figure 5. Geometry of the glass cylinder/vacuum vessel system.

The total angle subtended is divided by two here because the ϕ angle is measured from the vertical (z-axis) in the spherical coordinate system. Next, *SA* can be used to calculate the x-ray power at the source by using (7). A beryllium filter was used to prevent transmission of unwanted photons and charged particles to the detector (the detector's transmission curve is shown in Figure 6). Therefore, a transmission compensation factor is included in the x-ray power calculation.

$$P_{Xray} = V_{Os} \cdot \frac{1}{R_I} \cdot \frac{1}{\Re_{Xray}} \cdot \frac{1}{f_F} \cdot \frac{1}{A_D} \cdot SA \cdot \frac{1}{f_E} \ (W) \tag{7}$$

where V_{Os} = the voltage read from the oscilloscope (V), R_I = the oscilloscope input resistance (Ω), $\Re_{Xray}$ = the responsivity for the soft x-rays (A/W), f_F = the average transmission fraction through the Be filter, A_D = the surface area of the detector face (cm^2), *SA* = the surface area subtended by the hole (cm^2), and f_E = the fraction of x-rays escaping through the hole in the glass cylinder.
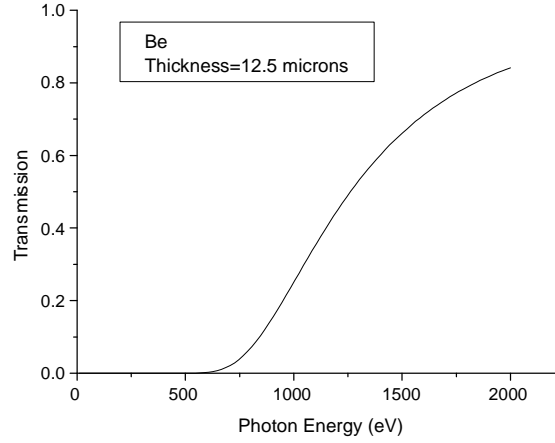
9

Figure 6. Beryllium filter transmission rate as a function of photon energy.

Note from Figure 6 that the Be window cuts off all x-rays below 600 V. Thus, as stressed earlier relative to Figure 4, the observed x-rays must have energies > 600 V (despite the ~ 300 V discharge energy). In view of Karabut's earlier work [1, 2], it seems logical that these x-rays have energy of ~ 1.5-2.0 keV.

Once the power is obtained, the intensity of the x-rays is simply

$$I_{Xray} = P_{Xray}A_T \ \ (W/cm^2) \tag{8}$$

where A_T = the exposed surface area of the target. Additionally, the dose over a pulse is defined as

$$D_{Xray} = \int I_{Xray}dt = I_{Xray}t_{Xray} \ \ (J/cm^2) \tag{9}$$

where t_{Xray} = the duration of the x-ray pulse. Finally, the x-ray production efficiency (x-ray power out/electrical power in) can be defined as

$$\eta_{Xray} = \frac{P_{Xray} \cdot t_{Xray}}{V_{in} \cdot I_{in} \cdot t_{in}} \cdot 100 \ \ (\%) \tag{10}$$

where V_{in} = the input voltage, I_{in} = the input current, and t_{in} = the duration of the input pulse. Values for the constants are listed in Table 4, while the calculated values for the x-ray power, intensity, dose, and efficiency are tabulated in Table 5.

Table 4. Constants required for the x-ray power, intensity, dose, and efficiency calculations.

Parameter	Symbol	Units	Value
Vessel radius	r	cm	27.5
Responsivity for soft x-rays	$\Re_{Xray}$	A/W	0.270
Be filter transmission fraction	f_F		0.75
Detector surface area	A_D	cm^2	1.0
X-ray escape fraction	f_E		0.05
Exposed target surface area	A_T	cm^2	1.0
Input voltage	V_{in}	V	250
Input current	I_{in}	A	1.5
Input pulse duration	t_{in}	ms	1

Assuming an x-ray quanta energy of $E_x = 1.3$ keV, the 13.4 mW/cm^2 intensity shown in Table 5 corresponds to 6.4×1013 q/s-cm^2. While the dose per pulse is small, the instantaneous x-ray power over the pulse is in the mW range. The x-ray efficiency is quite low, suggesting improved operation may be sought in future experiments.

Table 5. Calculated values for x-ray power, intensity, dose, and efficiency averaged over 3 measurements at 500 mTorr (see Figure 4).

Parameter	Symbol	Units	Value
Oscilloscope voltage	V_{Os}	mV	90.9
X-ray power	$P_{X\text{-}ray}$	mW	13.4
X-ray intensity	$I_{X\text{-}ray}$	mW/cm^2	13.4
X-ray pulse duration	$t_{X\text{-}ray}$	ms	0.263
X-ray dose	$D_{X\text{-}ray}$	µJ/cm^2	3.3
X-ray efficiency	$\eta_{X\text{-}ray}$	%	8.9×10^{-4}

6   Auxillary x-ray experiments using D-desorption

One theoretical explanation for these observations proposed by the authors is that the deuterium slows down in the target, diffuses, and accumulates in dislocation loops. If so, the diffusion time constant could account for the delay time before x-ray emission (Figure 4). X-ray emission from the high density in the "loop" cavities would explain the beamlet-like output reported by Karabut [1]-[2]. It is also consistent with the observation of a very high density of deuterium (~ metallic hydrogen) in dislocation loop areas which approach superconductivity conditions [6]. In view of this theory, an auxiliary D-desorption measurement was carried out. Pd:Dx cathodes were manufactured from the Pd foil used in the glow discharge experiments and loaded with deuterium by electrolysis (current density J = 10 mA/cm^2) to a concentration of x = D/Pd = 0.7. The deuterium was spontaneously evolved from the Pd:Dx cathode at room temperature. The TLD detectors were placed such as to partly cover the sample face. The TLDs were mated with polypropylene (PPE) filters 0-60 µm thick to obtain some energy resolution. The soft x-ray attenuation properties at very low x-ray energies were extrapolated below 4 keV from

existing data for polyethylene (PE), which is very similar to PPE. Results from the TLDs are presented in Figure 7.
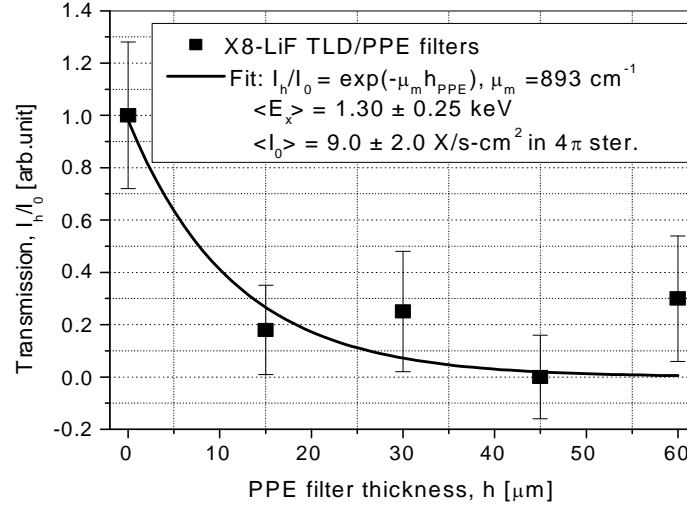

Figure 7. X-ray spectral measurements from a Pd:Dx cathode using a set of TLDs with PPE filters 0-60 µm thick.

Gamma-dosimetrical equations are used to analyze the TLD data. The total x-ray dose absorbed by a TLD having a surface area $S' = 0.04$ cm^2 and a thickness $h = 1$ mm can be expressed as:

$$D = \frac{\Phi_x E_x \mu_m S' \cdot 1.6 \times 10^{-13}}{\rho_{LiF}} \; (J\text{-}cm^2/MeV\text{-}kg) \qquad (11)$$

where Φ_x = the x-ray flux (cm^{-2}-s^{-1}), μ_m = the mass-absorption coefficient of a LiF TLD corresponding to the expected/measured x-ray quanta energy, and $\rho_{LiF} = 0.00262$ kg/cm^3 is the density of a LiF TLD unit. According to (11), knowledge of the absorbed dose D allows a calculation of either the x-ray flux Φ_x (if E_x is already determined) or the x-ray quanta energy E_x (if the flux is previously known). For our TLD experiments, an average E_x of 1.3 ± 0.25 keV was estimated from the x-ray transmission through the PPE filters shown in Figure 7. Then, the emission rate calculated from the TLDs data is about 9.0 photons/s-cm^2. As expected, due to the very small D flux obtained in desorption, this value is many orders of magnitude lower than the PGD case. However, the observation of soft x-rays in these auxiliary experiments provides added evidence for the proposal that the PGD x-ray emission involves D diffusion and desorption.

7   Conclusions

Strongly non-linear x-ray emission occurs and has been measured during intense D-bombardment of a Pd target using a pulsed deuterium discharge method. It is noted that there is a delay time preceding emission, but the key feature is that the x-ray energy E_x is greater than the discharge voltage. The PGD setup and diagnostics used in the experiment have been discussed in detail to aid others who may wish to adopt these techniques. Deuterium diffusion and desorption are thought to be vital steps in the x-ray emission mechanism. This seems consistent with the output data, and an auxiliary experiment provides supporting evidence.

References

1. A.B. Karabut, "Research into powerful solid x-ray laser with excitation of high current glow discharge ions," *Proceedings, 11th International Conference on Emerging Nuclear Energy Systems*, Albuquerque, NM, pp. 374-382, (2002).
2. G.H. Miley, A.G. Lipson and A. B. Karabut, "A new type of phonon-driven x-ray laser," *ICFA-6, Novel Accelerators and Laser-Beam Interactions*, Oxford, England, (2003).
3. P.B. Corkum, *Physical Review Letters* **71**, 001994 (1993).
4. International Radiation Detectors, Inc., "International Radiation Detectors, Inc.," Oct. 2005, http://www.ird-inc.com/frontpage.html.
5. Health Physics Society, "Radionuclide decay data," Oct. 2005, http://hps.org/publicinformation/radardecaydata.cfm.
6. A.G. Lipson, C.H. Castano, G.H. Miley, B. F. Lyakhov, A. Tsivadze, A. Yu., and A.V. Mitin, "Evidence of superstoichiometric H/D LENR active sites and high temperature superconductivity in a hydrogen-cycled Pd/PdO," *ICCF-12, International Conference on Condensed Matter Nuclear Science*, Yokohama, Japan, (2005).